Optimisation of alloy composition for highly-formable magnesium sheet

Zhuoran Zeng, Mingzhe Bian, Shiwei Xu, Weineng Tang, Chris Davies, Nick Birbilis, and Jianfeng Nie

View the article online at SpringerLink or IJMMM Webpage.

Articles you may be interested in

Semih Mahmut Aktarer, Dursun Murat Sekban, Tevfik Kucukomeroglu, and Gencaga Purcek, Microstructure, mechanical properties and formability of friction stir welded dissimilar materials of IF-steel and 6061 Al alloy, *Int. J. Miner. Metall. Mater.*, 26(2019), No. 6, pp. 722-731. https://doi.org/10.1007/s12613-019-1783-z

Xiao-feng Wang, Ming-xing Guo, Cun-qiang Ma, Jian-bin Chen, Ji-shan Zhang, and Lin-zhong Zhuang, Effect of particle size distribution on the microstructure, texture, and mechanical properties of Al–Mg–Si–Cu alloy, *Int. J. Miner. Metall. Mater.*, 25(2018), No. 8, pp. 957-966. https://doi.org/10.1007/s12613-018-1645-0

Chang-qing Huang, Jia-xing Liu, and Xiao-dong Jia, Effect of thermal deformation parameters on the microstructure, texture, and microhardness of 5754 aluminum alloy, *Int. J. Miner. Metall. Mater.*, 26(2019), No. 9, pp. 1140-1150. https://doi.org/10.1007/s12613-019-1852-3

Hai-jun Wang, Zhe Rong, Li Xiang, Sheng-tao Qiu, Jian-xin Li, and Ting-liang Dong, Effect of decarburization annealing temperature and time on the carbon content, microstructure, and texture of grain-oriented pure iron, *Int. J. Miner. Metall. Mater.*, 24(2017), No. 4, pp. 393-400. https://doi.org/10.1007/s12613-017-1419-0

L. Romero-Reséndiz, A. Flores-Rivera, I.A. Figueroa, C. Braham, C. Reyes-Ruiz, I. Alfonso, and G. González, Effect of the initial ECAP passes on crystal texture and residual stresses of 5083 aluminum alloy, *Int. J. Miner. Metall. Mater.*, 27(2020), No. 6, pp. 801-808. https://doi.org/10.1007/s12613-020-2017-0

Hong-tao Liu, Ji-xue Zhou, Dong-qing Zhao, Yun-teng Liu, Jian-hua Wu, Yuan-sheng Yang, Bai-chang Ma, and Hai-hua Zhuang, Characteristics of AZ31 Mg alloy joint using automatic TIG welding, *Int. J. Miner. Metall. Mater.*, 24(2017), No. 1, pp. 102-108. https://doi.org/10.1007/s12613-017-1383-8

IJMMM WeChat   QQ author group

Optimisation of alloy composition for highly-formable magnesium sheet

Zhuoran Zeng[1,2,✉], *Mingzhe Bian*[2], *Shiwei Xu*[3,4,✉], *Weineng Tang*[4], *Chris Davies*[5], *Nick Birbilis*[1], *and Jianfeng Nie*[2,✉]

1) College of Engineering and Computer Science, Australian National University, ACT. 2601, Australia
2) Department of Materials Science and Engineering, Monash University, VIC 3800, Australia
3) State Key Laboratory of Advanced Design and Manufacturing for Vehicle Body, Hunan University, Changsha 410082, China
4) Research Institute (R & D Center), Baosteel Group Corporation, Shanghai 201999, China
5) Department of Mechanical and Aerospace Engineering, Monash University, VIC 3800, Australia

Abstract: The effectiveness of Ca or Gd addition on ductility and formability of Mg–Zn–Zr based dilute alloys in deep drawing has not been systematically compared previously. In this study, formable Mg–Zn–Gd–Zr and Mg–Zn–Ca–Zr sheet alloys are produced by hot rolling. These sheets have similarly weakened basal texture, but the sheet of the Mg–Zn–Gd–Zr alloys has higher ductility and formability than that of Mg–Zn–Ca–Zr alloys. The combined addition of 0.2wt% Ca and 0.4wt% Gd to the Mg–1Zn–0.5Zr (wt%) alloy leads to a Mg–1Zn–0.4Gd–0.2Ca–0.5Zr alloy that has even better ductility, and its formability during deep drawing is comparable to the benchmark Al6016 sheet. An increase in Ca content from 0.2wt% to 0.5wt% leads to decreased sheet ductility and formability, predominantly due to grain boundary embrittlement.

Keywords: magnesium sheet alloy; texture; microstructure; formability; solute segregation

1. Introduction

Magnesium (Mg) and its alloys are the lightest metallic structural material, and the development of high-performance Mg alloys has been stimulated by the requirement of weight-saving in the automotive, aerospace, and communications industries [1–2]. Despite the significance of Mg alloys as a class of engineering materials, the adoption of Mg rolling sheets in industrial applications remains limited compared to that achieved for Al sheets. Commercial Mg alloy AZ31 (Mg–3wt%Al–1wt%Zn) has inadequate formability and ductility at near room temperatures [3–4]. The formability of AZ31 sheet, indicated by bi-axial stretching (Erichsen) test, is about 3–4 [5–6], whilst the formability of Al sheet alloys is about 8–10 [7]. With respect to deep drawing, the drawability at room temperature, represented by the limit drawing ratio (LDR), is quite low for Mg sheet, e.g., about 1.3–1.7 for AZ31 [8–9], whilst the LDR for Al, copper, and brass sheets at room temperature are about 2.2–2.5 [10]. The poor formability of Mg sheet is caused by an insufficient number of deformation modes that is caused by its hexagonal crystal structure and a strong crystallographic texture developed during rolling [11].

In the past two decades, considerable effort has been made to develop formable Mg alloy sheets via the texture weakening approach. It was found that the strong crystallographic texture, i.e., [0001]//ND (normal direction) of the rolled sheet, can be weakened by the addition of Ca or RE (rare-earth element) and in combination [12–13]. The combined addition of Zn/Ca or Zn/RE causes an even weaker texture, in which the major texture component is split and tilted toward the transverse direction (TD), known as TD-split texture [13–18]. Consequently, the commercial alloy ZEK100 (Mg–1Zn–0.2Nd–0.2Zr) has demonstrated a great improved rollability and formability compared with conventional Mg–Al-based sheet alloys [14,19], in which Zr is added to refine grain size. Whilst numerous studies have reported the texture weakening and the resultant improvement in ductility and sketch formability in Mg–Zn–RE and Mg–Zn–Ca alloys [13–18], systematic comparison of the ductility and formability, especially deep-drawability, of these Mg–Zn-base sheets alloys, has not been reported yet. Hence, so far it is still not clear if there is an optimum combination of alloying additions that gives rise to optimised formability.

To solve these issues, we investigated 7 alloys based on the Mg–Zn–Gd–Zr and Mg–Zn–Ca(–Zr) systems. For consistency, they were thermomechanically processed under similar conditions. The alloying elements Zn, Gd, and Ca were added in different combinations. As aforementioned, Zn, Gd, and Ca were added to control the basal texture and

🙆 Springer

achieve higher formability. Alloy compositions are listed in Table 1. Whilst the Ca effect in Mg–Ca binary alloys has been revealed in a previous study [20], the effect of Ca content on alloy formability in the Mg–Zn–Ca ternary system is still unclear, but this can be revealed by comparing Mg–1Zn–0.2Ca and Mg–1Zn–0.5Ca alloys. Whilst Zr was known to refine the grain size, whether Zr addition will change the sheet formability in the Mg–Zn–Ca system was not clear. This can be illustrated by comparing the Mg–1Zn–0.5Ca and Mg–1Zn–0.5Ca–0.5Zr alloy. The investigation of Mg–1Zn–0.5Ca–0.4Gd alloy is to show whether the addition of Gd to Mg–Zn–Ca can further enhance alloy formability; whilst the comparison between Mg–1Zn–0.4Gd–0.5Zr and

Mg–1Zn–0.5Ca–0.5Zr is to illustrate which element, Gd or Ca, is more effective in enhancing alloy formability in the Mg–Zn–Zr system, as both Gd and Ca are known to weaken basal texture and increase formability. The addition of 0.2wt% Ca and 0.5wt% Ca to Mg–1Zn–0.4Gd–0.5Zr is to verify whether dilute addition of Ca to Mg–Zn–Gd–Zr system can affect alloy formability, and to address the role of Ca content. In this study, Mg–3Al–1Zn–0.3Mn (AZ31) and Al6016-T4 alloy sheets were the benchmarks. By comparing sheet ductility and formability among the studied alloys and with the benchmarks, the effect of each element on ductility and formability is demonstrated in this work, and the optimum combination is revealed.

Table 1.   Nominal and measured compositions of the alloys in the present study

Alloy system	Nominal composition / wt%	Measured composition / wt%
Mg–Zn–Ca	Mg–1Zn–0.2Ca	Mg–0.98Zn–0.19Ca
	Mg–1Zn–0.5Ca	Mg–0.95Zn–0.46Ca
	Mg–1Zn–0.5Ca–0.5Zr	Mg–1.03Zn–0.49Ca–0.29Zr
	Mg–1Zn–0.5Ca–0.4Gd	Mg–0.95Zn–0.46Ca–0.39Gd
Mg–Zn–Gd	Mg–1Zn–0.4Gd–0.5Zr	Mg–1.00Zn–0.44Gd–0.43Zr
	Mg–1Zn–0.4Gd–0.2Ca–0.5Zr	Mg–0.98Zn–0.44Gd–0.19Ca–0.49Zr
	Mg–1Zn–0.4Gd–0.5Ca–0.5Zr	Mg–1.01Zn–0.42Gd–0.47Ca–0.39Zr
Benchmark	Mg–3Al–1Zn–0.3Mn (AZ31)	Mg–3.06Al–0.78Zn–0.45Mn
	Al–1.2Si–0.4Mg (Al6016)	—

2. Experimental

Alloys in Table 1 were cast at 760°C under an inert (argon) atmosphere with R134a gas, followed by 400°C homogenisation for 24 h. Homogenised alloys were hot-rolled from 5 to 1 mm by 8 passes at 450°C, and annealed at 400°C for 30 min. To measure the alloy composition, the samples were digested in a mixture of hydrochloric acid and nitric acid. These solutions were analysed using a Varian 730ES optical emission spectrometer. Tensile test specimens were prepared from annealed sheets along the rolling direction (RD) with the gauge length of 10 mm and a width of 5 mm. Surfaces of tensile specimens were metallographically prepared using SiC paper prior to each test. Specimens of each condition were tested twice, with tensile testing performed in an Instron 4505 tensile test machine at room temperature, with an initial strain rate of 0.001 s^{-1}. Sheet deep drawability was measured using mini swift method [21–22]. The samples were a set of round discs of diameters 9, 9.5, 10, 10.5, 11.5, 13.1, and 14.6 mm. These samples were punched from the as-annealed sheets and ground to 0.5 mm in thickness. The flat discs were placed on the die, which was installed in the Instron 4505 mechanical testing machine as shown in Fig. 1. Once the testing started, the flat disc would be deep drawn into the die by a punch, whose diameter is 6 mm, in a constant speed at 0.5 mm/min. Using the mini deep drawing test, the LDR of each sheet alloy was determined. LDR is defined as the ratio of the largest disc in diameter that could be drawn without cracking to the punch diameter. A larger LDR value represents the better formability of the alloy sheet.
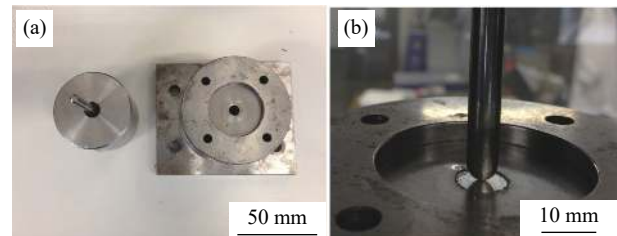
Fig. 1.   Photos showing (a) punch and die for deep-drawing test and (b) punch just touching blank disc that was aligned above die cavity without blank holder (for demonstration purpose).

Scanning electron microscopy (SEM) and electron backscatter diffraction (EBSD) were used to observe the texture and surface features, such as slip traces and cracks. The samples for SEM and EBSD were metallographically prepared using 4000-grit SiC papers, 50 nm-diameter silica suspension, and ion polishing using Gatan precision etching and coating system (PECS™). SEM and EBSD were performed using a FEI Quanta 3D-FEG scanning electron microscope equipped with a Pegasus Hikari EBSD detector. EBSD scan was performed with an accelerating voltage of 25 kV and beam current of 23 nA and at the step of 0.2 μm. High-angle annular dark-field scanning transmission electron microscopy (HAADF-STEM) and energy-dispersive X-ray spectroscopy (EDS) were performed in a FEI F20 transmission electron microscope operating at 200 kV. The specimens for STEM were 3 mm diameter discs, and they were mechanically thinned to 0.06 mm, and ion-polished using Gatan preci-

sion ion polishing system (PIPS II™, voltage 4.8 kV and angle 4°) at −60°C until a small hole formed in the specimen.

3. Results

Fig. 2 shows the microstructure and texture of the as-annealed alloy sheets. The Mg–Zn–Ca(–Zr) and Mg–Zn–Gd–Zr alloy sheets had equiaxed grains and weakened basal texture. The basal pole of samples was split and tilted toward the TD. The texture intensities varied a little bit, in the range of 2.7–4.6 multiples of random distribution (mrd). In contrast, the AZ31 sheet has a much stronger basal texture (8.8 mrd), whose major (0001) texture pole was along ND. The Mg–1Zn–0.2Ca alloy had the largest grain size of 37.5 μm in diameter, which was reduced to 23.9 μm by increasing Ca content from 0.2wt% to 0.5wt%. A greater refinement in grain size was achieved by Zr alloying addition; the grain size of Mg–1Zn–0.5Ca–0.5Zr alloy was 11.2 μm, less than half of that of the Zr-free counterpart. In contrast, the dilute addition of 0.4wt% Gd to Mg–1Zn–0.5Ca could not decrease the

grain size. The grain size of Mg–1Zn–0.4Gd–0.5Zr was 16.3 μm, larger than that of the Mg–1Zn–0.5Ca–0.5Zr alloy. The Ca alloying further decreased the grain size to 11.8 μm after 0.2wt% Ca addition, and 8.5 μm after 0.5wt% Ca addition. These observations suggested that Zr and Ca additions are effective in refining the grains, but such refinement from Gd is limited.

Fig. 3(a) and (b) show tensile stress–strain curves of the as-annealed sheets and benchmarks. Tensile properties, including yield strength, tensile strength, uniform elongation, total elongation, and strain hardening exponent, along the rolling direction, are summarised in Table 2. The Mg–1Zn–0.2Ca alloy had a low yield strength of 111 MPa. A higher Ca content of 0.5wt% increased the yield strength to 129 MPa, whilst the Zr addition further increased the yield strength to 158 MPa. Such strengthening did not compromise ductility, as the total elongations of these three alloys were 27%–28%. In contrast, the addition of Gd to Mg–1Zn–0.5Ca alloy decreased the alloy strength to 113 MPa but increased the total elongation to 30%.
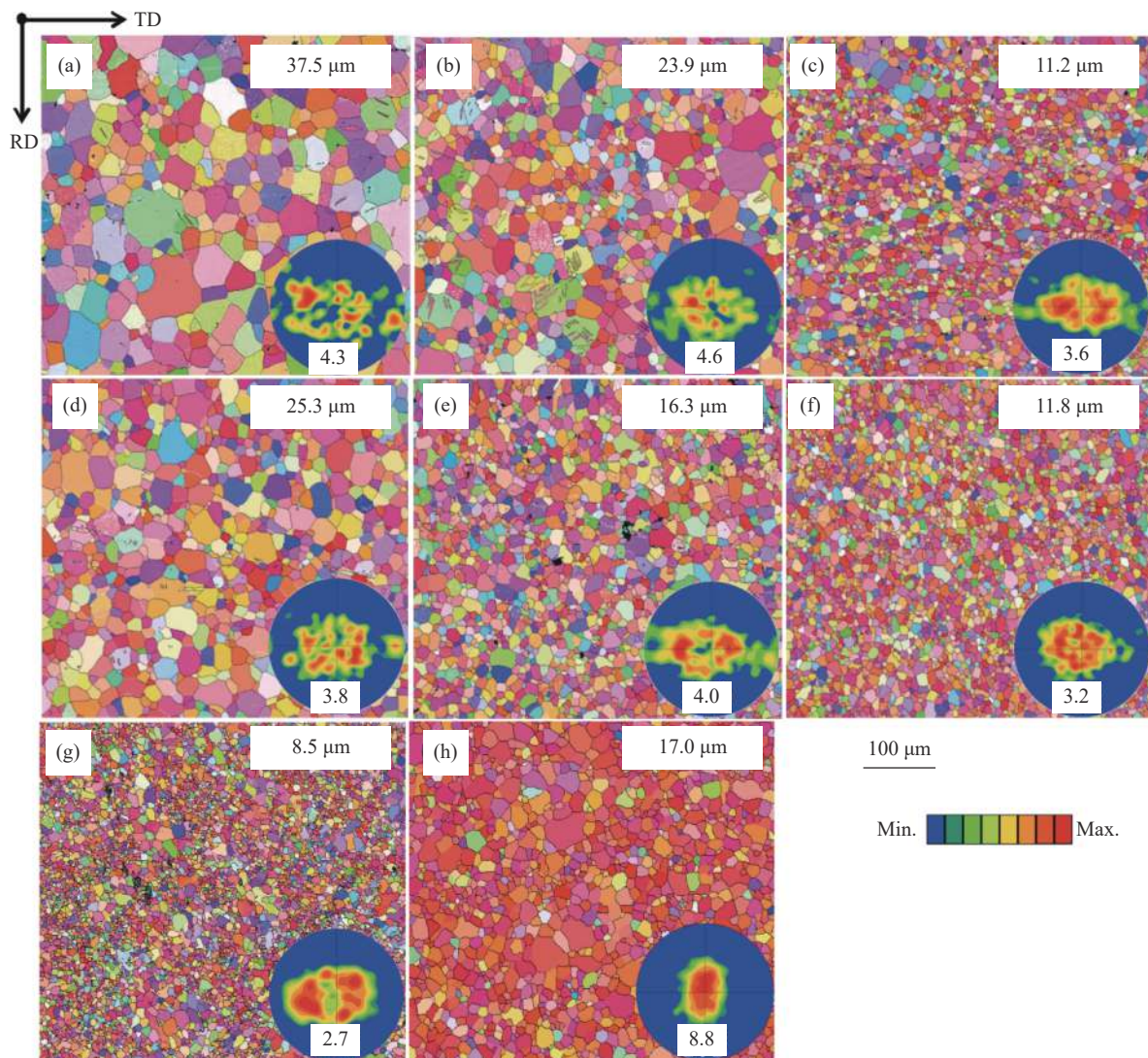
Fig. 2. EBSD orientation maps and corresponding (0001) pole figures showing microstructure and texture of as-annealed sheets of (a) Mg–1Zn–0.2Ca, (b) Mg–1Zn–0.5Ca, (c) Mg–1Zn–0.5Ca–0.5Zr, (d) Mg–1Zn–0.5Ca–0.4Gd, (e) Mg–1Zn–0.4Gd–0.5Zr, (f) Mg–1Zn–0.4Gd–0.2Ca–0.5Zr, (g) Mg–1Zn–0.4Gd–0.5Ca–0.5Zr, and (h) benchmark AZ31 sheet. Grain sizes are provided.
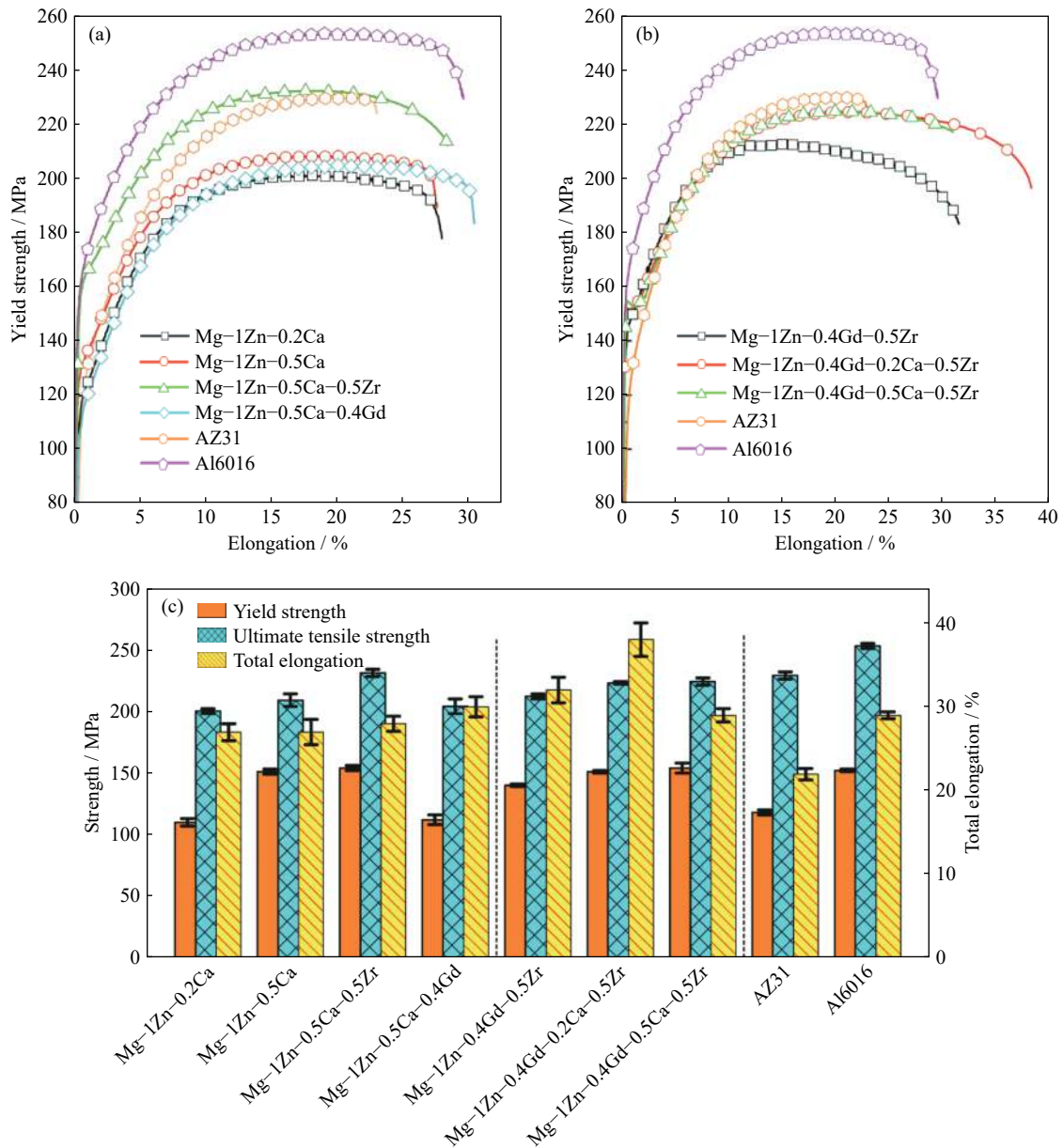
Fig. 3.   Tensile tests of sheets of (a) Mg–Zn–Ca(–Zr) alloys and (b) Mg–Zn–Gd–Zr. (c) Bar chart summarising yield strength and ductility of the alloy sheets.

Table 2.   Tensile tests along the rolling direction and mini-deep drawing test results of Mg–Zn–Ca(–Zr) and Mg–Zn–Gd–Zr alloys sheets and benchmark AZ31 and Al6016

Composition	Yield strength / MPa	Tensile strength / MPa	Uniform elongation / %	Total elongation / %	Strain hardening exponent	LDR
Mg–1Zn–0.2Ca	111 ± 3	201 ± 2	17 ± 1	27 ± 1	0.24 ± 0.01	1.86 ± 0.04
Mg–1Zn–0.5Ca	129 ± 2	210 ± 5	18 ± 0.4	27 ± 1.5	0.22 ± 0.005	1.88 ± 0.02
Mg–1Zn–0.5Ca–0.5Zr	158 ± 2	232 ± 3	18 ± 0.7	28 ± 0.9	0.20 ± 0.008	1.89 ± 0.01
Mg–1Zn–0.5Ca–0.4Gd	113 ± 4	205 ± 6	19 ± 0.2	30 ± 1.2	0.25 ± 0.012	1.86 ± 0.03
Mg–1Zn–0.4Gd–0.5Zr	141 ± 1	213 ± 2	19 ± 0.3	32 ± 1.5	0.19 ± 0.007	1.91 ± 0.02
Mg–1Zn–0.4Gd–0.2Ca–0.5Zr	152 ± 1	224 ± 1	20 ± 0.1	38 ± 2.0	0.22 ± 0.004	1.97 ± 0.03
Mg–1Zn–0.4Gd–0.5Ca–0.5Zr	155 ± 4	225 ± 3	21 ± 0.5	29 ± 0.8	0.23 ± 0.013	1.81 ± 0.02
Mg–3Al–1Zn–0.3Mn (AZ31)	119 ± 2	230 ± 3	20 ± 0.1	22 ± 0.7	0.27 ± 0.01	1.62 ± 0.05
Al–1.2Si–0.4Mg (Al6016)	153 ± 1	254 ± 2	20 ± 0.1	29 ± 0.4	0.28 ± 0.006	1.94 ± 0.02

   The Mg–1Zn–0.4Gd–0.5Zr alloy had a lower yield strength (141 MPa) but a higher ductility (32%) than the Mg–1Zn–0.5Ca–0.5Zr counterpart. The 0.2wt% Ca addition

to Mg–1Zn–0.4Gd–0.5Zr alloy resulted in an increase in yield strength from 141 to 152 MPa. More importantly, with the 0.2wt% Ca addition, the ductility was significantly en-

1392

Int. J. Miner. Metall. Mater., Vol. 29, No. 7, Jul. 2022

hanced from 32% to 38%. Such enhancement in both ductility and strength makes Mg–1Zn–0.4Gd–0.2Ca–0.5Zr alloy overwhelmingly superior to AZ31, and competitive to Al6016-T4. When the Ca content increased from 0.2wt% to 0.5wt% (Mg–1Zn–0.4Gd–0.5Ca–0.5Zr alloy), the total elongation decreased from 38% to 29%, while the strength and uniform elongation were almost unchanged.

The formability of alloy sheets was measured by mini deep drawing test. During the deep drawing process, discs with larger diameter are more difficult to be fully deep drawn without any visible cracks. Fig. 4(a) shows that the Mg–1Zn–0.4Gd–0.5Zr sample with 10 mm diameter was fully deep drawn, while the samples with diameter of 11.5 mm and 14.6 mm were cracked. The deep drawing results depend on alloy composition. For example, although the Mg–1Zn–0.4Gd–0.2Ca–0.5Zr and AZ31 samples had the same diameter, 11.5 mm, the Mg–1Zn–0.4Gd–0.2Ca–0.5Zr alloy was fully deep-drawn but the AZ31 alloy was cracked (Fig. 4(b)).

LDR was used here to quantitatively interpret formability obtained from the mini deep drawing test. Taking Mg–1Zn–0.4Gd–0.5Zr sheet as an example, the disc samples with 9, 9.5, 10, and 10.5 mm diameters were fully deep drawn, whilst the samples, whose diameters were larger than 10.5 mm, were cracked during the mini deep drawing test. Due to strain hardening, the load continuously increased with punch displacement. After the sample was fully drawn into the die, the load would gradually decrease with the further punch displacement. If a crack generates, then the load drops dramatically and a sharp inflection point could be found in the load–displacement curve. Based on the load–displacement curves (Fig. 4(c)), the ratio of the diameter of blank (D) to the diameter of punch (d), i.e., D/d, and the maximum load of each sample were both recorded as a (x, y) datum point in the plot shown in Fig. 4(d). LDR was calculated from the projected value along the x-axis of the point that the straight line fitted from the data points of cracked samples intersected with the straight line fitted from the data points of fully drawn samples. As indicated by Fig. 4(d), the LDR of the Mg–1Zn–0.4Gd–0.5Zr alloy was 1.91 at room temperature.
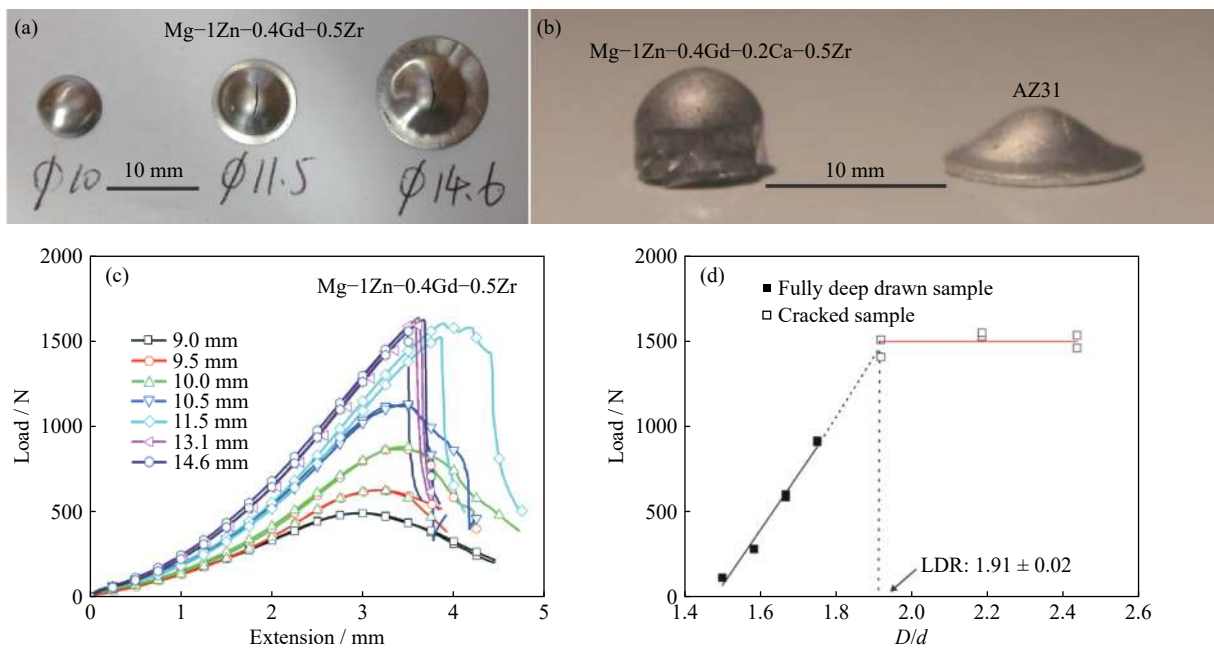
Fig. 4. Photos of (a) Mg–1Zn–0.4Ca–0.5Zr samples after deep-drawing from blank disc with different sizes (10, 11.5, and 14.6 mm) and (b) Mg–1Zn–0.4Gd–0.2Ca–0.5Zr and AZ31 samples with the same blank diameter (11.5 mm) after deep drawing. (c) Load–extension curves of Mg–1Zn–0.4Gd–0.5Zr samples and (d) LDR measured at room temperature. Filled squares represent data points of fully drawn samples without any visible cracks, while hollow squares are data points of cracked samples.

Fig. 5 shows the LDR values of the alloy sheets, allowing their formability to be compared. The Mg–Zn–Ca(–Zr) based alloys had similar LDR values between 1.86 and 1.89, which were significantly higher than the benchmark AZ31 alloy (1.62) but still lower than the benchmark Al alloy (1.94). In the Mg–Zn–Gd–Zr system, the Mg–1Zn–0.4Gd–0.5Zr alloy had a similar LDR value to Mg–1Zn–0.5Ca–0.5Zr counterpart. After dilute alloying of 0.2wt% Ca, the alloy formability increased significantly. The Mg–1Zn–0.4Gd–0.2Ca–0.5Zr alloy had the best formability among these sheets. The 11.5 mm diameter sample of only Mg–1Zn–0.4Gd–0.2Ca–0.5Zr and Al6016-T4 were fully deep drawn without cracking. The LDR value of Mg–1Zn–0.4Gd–0.2Ca–0.5Zr alloy was as large as 1.97, comparable to the Al6016 sheet in the present study. However, if the Ca content in the Mg–Zn–Gd–Zr based alloys increased from 0.2wt% to 0.5wt%, the formability of alloy decreased significantly. The LDR value of Mg–1Zn–0.4Gd–0.5Ca–0.5Zr alloy was only 1.8, which was even lower than the alloys without Ca addition (Mg–1Zn–0.4Gd–0.5Zr).

4. Discussion

By comparing the alloy ductility and formability, it is ob-
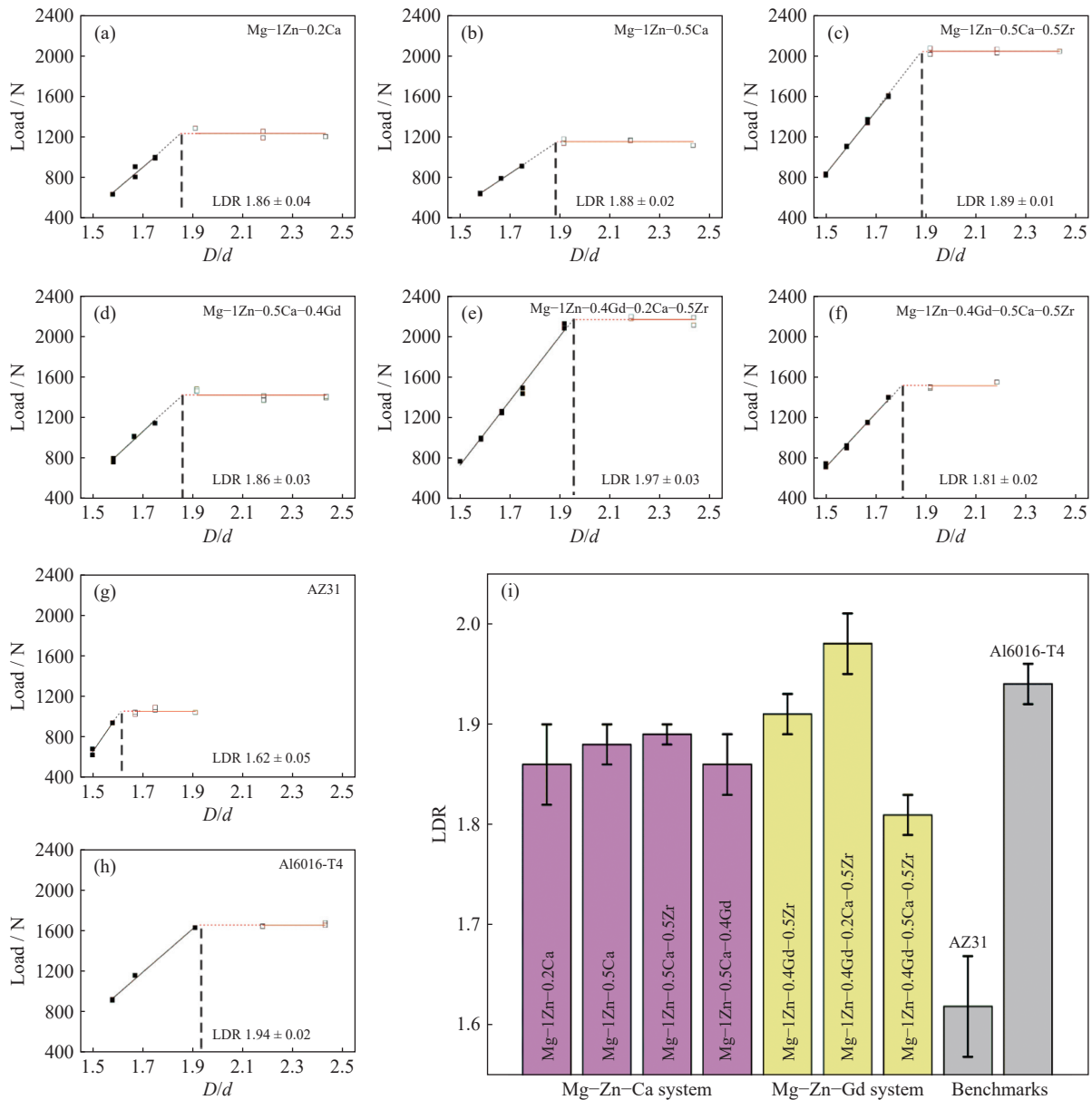
Fig. 5. Measured LDR of (a) Mg–1Zn–0.2Ca, (b) Mg–1Zn–0.5Ca, (c) Mg–1Zn–0.5Ca–0.5Zr, (d) Mg–1Zn–0.5Ca–0.4Gd, (e) Mg–1Zn–0.4Gd–0.2Ca–0.5Zr, (f) Mg–1Zn–0.4Gd–0.5Ca–0.5Zr, (g) AZ31, and (h) Al6016-T4 alloys. (i) Bar chart summarising the LDR values of the alloys, with respect to those of AZ31 and Al6016-T4 alloys.

vious that the Gd addition is more effective in enhancing alloy ductility, although either Gd or Ca addition to the Mg–1Zn-based alloys can lead to similar weakened TD-split texture. When Gd and Ca are added together, the texture weakening effect can be further enhanced. Such enhanced texture weakening by combined addition of RE and Ca was also observed when 0.1wt% Ca was added to Mg–4Zn–1MM (mischmetal) rolled sheet [23]. However, the improvement in ductility is essentially depending on Ca content. When the Ca content is low, e.g., 0.2wt% in the Mg–1Zn–0.4Gd–0.2Ca–0.5Zr alloy, the enhancement in ductility and formability can be quite significant compared with the Ca-free sheet. However, when the Ca content is increased to 0.5wt%, e.g., in the Mg–1Zn–0.4Gd–0.5Ca–0.5Zr or Mg–1Zn–0.5Ca–0.4Gd alloy, sheet ductility and formability become lower even than those of the Ca-free sheet. In order to figure out the reason for the decreased ductility, the surface of Mg–1Zn–

0.4Gd–0.2Ca–0.5Zr and Mg–1Zn–0.4Gd–0.5Ca–0.5Zr alloy sheets was examined after large elongation by 20% and 25% (Fig. 6(a)–(d)). Significant grain boundary cracking is observed in the Mg–1Zn–0.4Gd–0.5Ca–0.5Zr alloy when the elongation is 20% and above. In contrast, grain boundary cracks are invisible in the Mg–1Zn–0.4Gd–0.2Ca–0.5Zr alloy.

To reveal the origin of the observed difference in grain boundary cracking, the grain boundaries of the Mg–1Zn–0.4Gd–0.2Ca–0.5Zr and Mg–1Zn–0.4Gd–0.5Ca–0.5Zr were characterised using EDS–STEM (Fig. 7). In both alloys, the segregation of Zn and Gd atoms to grain boundaries is obvious. Such co-segregation of larger atoms (Gd) and smaller atoms (Zn) was speculated to result in texture weakening during recrystallisation [13]. However, the segregation of Ca to the grain boundary in the Mg–1Zn–0.4Gd–0.2Ca–0.5Zr alloy was quite weak, and only some segments of grain boundaries

1394

Int. J. Miner. Metall. Mater., Vol. 29, No. 7, Jul. 2022
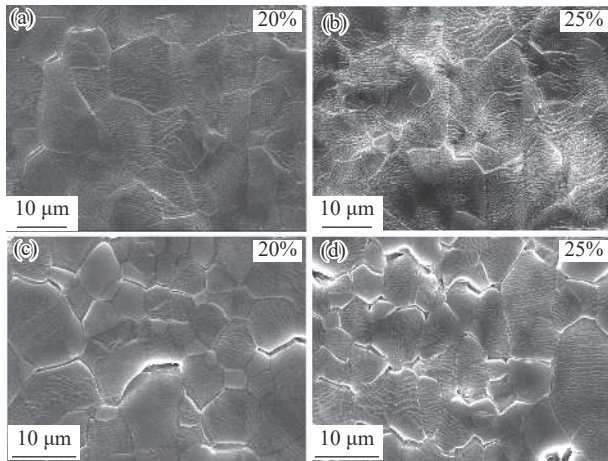
Fig. 6. SEM micrographs of (a, b) Mg–1Zn–0.4Gd–0.2Ca–0.5Zr and (c, d) Mg–1Zn–0.4Gd–0.5Ca–0.5Zr samples after 20% and 25% elongation.

had higher Ca content than the matrix. As a comparison, the segregation of Ca to grain boundaries is much more apparent in the Mg–1Zn–0.4Gd–0.5Ca–0.5Zr alloy. It is known that the grain boundary of Mg may become embrittled when elements with large atomic size but low solubility in Mg, such as Ca [20,24] and Na [25–26], are present in the boundary. More importantly, second phase particles were observed in the Mg–1Zn–0.4Gd–0.5Ca–0.5Zr alloy. The embrittlement of grain boundaries during uniaxial tensile testing caused by grain boundary precipitates and inclusions was reported, due to introducing stress concentration on grain boundary [27]. Whilst the dilute addition of Ca to Mg–Zn binary alloy can

increase grain boundary cohesion and reduce grain boundary cracking [20,24,28], the experimental results suggest that in the Mg–Zn–Gd-based alloy, the excessive Ca addition still embrittle grain boundary and reduce sheet formability even in formable Mg–Zn–Gd–Zr-based alloy. The critical Ca content should be lower than 0.5wt% to avoid the formation of grain boundary intermetallics.

This study also shows grain refinement induced by Zr and Ca additions. Ca has a low solubility in Mg and Zr even a lower. Therefore, the driving force to form intermetallic particles is higher in the case with Ca and Zr. These fine particles can act as nucleus for new grains and can reduces the grain grows by suppressing grain boundary movements during hot rolling and annealing [29]. This will change the recrystallization with an effect on the grain size of the rolling sheet. In contrast, Gd has much large solubility, and dilute addition of Gd does not result in the formation of intermetallic particles, and therefore, the grain size of Mg–1Zn–0.5Ca–0.4Gd is very similar to that of Mg–1Zn–0.5Ca alloy. Whilst the refined grain size due to Ca and Zr addition enhances alloy strength, the formability does not improve as a consequence predominantly, because (i) all the Mg–Zn based alloys herein have similarly weakened basal texture, and (ii) intragranular dislocation slip is still the dominant deformation mode with the grain size of ~10–20 μm. It is speculated that when the grain size of these dilute alloys are refined to ~1 μm or submicron, the formability would be increased substantially due to the operation of intergranular deformation modes such as grain boundary sliding [30–31].
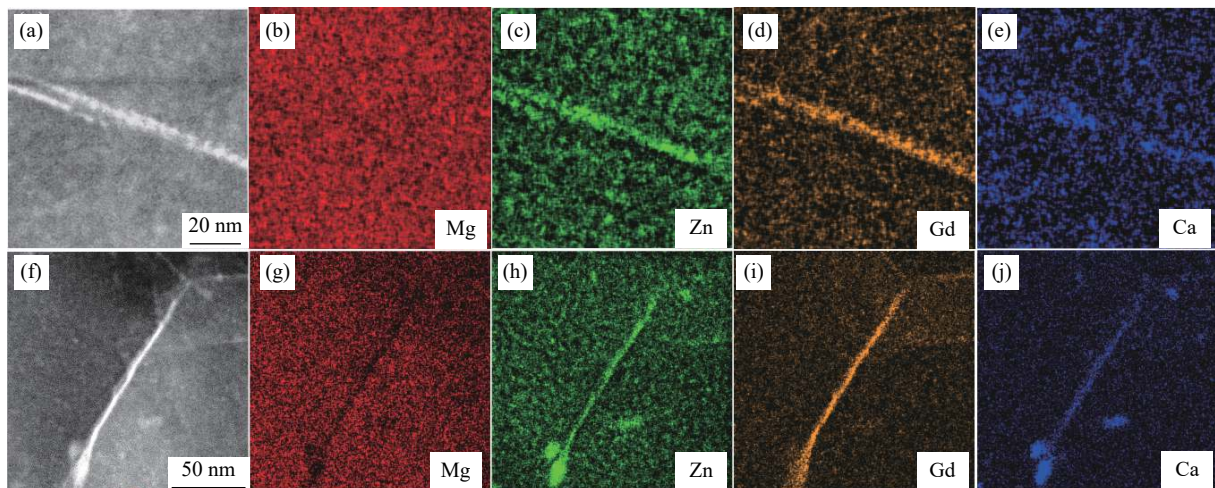
Fig. 7. HAADF-STEM and corresponding EDS mapping showing element distribution in the grain boundary region of (a–e) Mg–1Zn–0.4Gd–0.2Ca–0.5Zr and (f–j) Mg–1Zn–0.4Gd–0.5Ca–0.5Zr samples in the as-annealed state.

5. Conclusions

In this study, the formability of Mg–Zn–Ca(–Zr) and Mg–Zn–Gd–Zr sheet alloys were assessed by tensile tests and mini-deep drawing tests, and their microstructures were characterised by electron microscopy. The main conclusions were drawn as follows:

(1) The addition of Gd or Ca in the Mg–Zn-based alloy

weakened sheet basal texture and enhanced alloy formability compared with benchmark AZ31, but Gd addition was more effective in improving alloy formability than Ca addition.

(2) Dilute addition of Ca (0.2wt%) to Mg–1Zn–0.4Gd–0.5Zr alloy significantly enhanced the alloy ductility and formability, which is comparable to that of the Al6016-T4 sheet in the mini deep drawing tests.

(3) With an increase in Ca content to 0.5wt%, sheet ductil-

ity and formability decreased, predominantly due to grain boundary embrittlement. This is speculated to be caused by more significant grain boundary segregation of Ca atoms and the formation of intermetallic particles in grain boundaries.

(4) The Zr addition refined grain size and increased alloy strength, but did not enhance alloy formability substantially.

Acknowledgements

Conflict of Interest

The authors declare no competing financial and non-financial interests.

References

[1] W.J. Joost and P.E. Krajewski, Towards magnesium alloys for high-volume automotive applications, *Scripta Mater.*, 128(2017), p. 107.

[2] T.M. Pollock, Weight loss with magnesium alloys, *Science*, 328(2010), No. 5981, p. 986.

[3] S. Yi, J. Bohlen, F. Heinemann, and D. Letzig, Mechanical anisotropy and deep drawing behaviour of AZ31 and ZE10 magnesium alloy sheets, *Acta Mater.*, 58(2010), No. 2, p. 592.

[4] N. Stanford and M. Barnett, Effect of composition on the texture and deformation behaviour of wrought Mg alloys, *Scripta Mater.*, 58(2008), No. 3, p. 179.

[5] Y. Chino and M. Mabuchi, Enhanced stretch formability of Mg–Al–Zn alloy sheets rolled at high temperature (723 K), *Scripta Mater.*, 60(2009), No. 6, p. 447.

[6] B.C. Suh, M.S. Shim, K.S. Shin, and N.J. Kim, Current issues in magnesium sheet alloys: Where do we go from here? *Scripta Mater.*, 84-85(2014), p. 1.

[7] Y. Chino, K. Sassa, and M. Mabuchi, Tensile properties and stretch formability of Mg–1.5 mass%–0.2 mass%Ce sheet rolled at 723 K, *Mater. Trans.*, 49(2008), No. 7, p. 1710.

[8] K.F. Zhang, D.L. Yin, and D.Z. Wu, Formability of AZ31 magnesium alloy sheets at warm working conditions, *Int. J. Mach. Tools Manuf.*, 46(2006), No. 11, p. 1276.

[9] K.I. Mori and H. Tsuji, Cold deep drawing of commercial magnesium alloy sheets, *J. Jpn. Soc. Technol. Plast.*, 48(2007), No. 552, p. 41.

[10] G. Dieter, *Mechanical Metallurgy*, 3rd ed., McGrow-Hill, London, 1986, p. 672.

[11] I. Polmear, D. StJohn, J.F. Nie, and M. Qian, Magnesium alloys, [in] *Light Alloys: Metallurgy of the Light Metals*, 5th ed., Butterworth-Heinemann, Oxford, 2017, p. 287.

[12] K. Hantzsche, J. Bohlen, J. Wendt, K.U. Kainer, S.B. Yi, and D. Letzig, Effect of rare earth additions on microstructure and texture development of magnesium alloy sheets, *Scripta Mater.*, 63(2010), No. 7, p. 725.

[13] Z.R. Zeng, Y.M. Zhu, S.W. Xu, M.Z. Bian, C.H.J. Davies, N. Birbilis, and J.F. Nie, Texture evolution during static recrystal-

lization of cold-rolled magnesium alloys, *Acta Mater.*, 105(2016), p. 479.

[14] J. Bohlen, M.R. Nürnberg, J.W. Senn, D. Letzig, and S.R. Agnew, The texture and anisotropy of magnesium–zinc–rare earth alloy sheets, *Acta Mater.*, 55(2007), No. 6, p. 2101.

[15] I. Basu and T. Al-Samman, Triggering rare earth texture modification in magnesium alloys by addition of zinc and zirconium, *Acta Mater.*, 67(2014), p. 116.

[16] Y. Chino, T. Ueda, Y. Otomatsu, K. Sassa, X.S. Huang, K. Suzuki, and M. Mabuchi, Effects of Ca on tensile properties and stretch formability at room temperature in Mg–Zn and Mg–Al alloys, *Mater. Trans.*, 52(2011), No. 7, p. 1477.

[17] J. Hirsch and T. Al-Samman, Superior light metals by texture engineering: Optimized aluminum and magnesium alloys for automotive applications, *Acta Mater.*, 61(2013), No. 3, p. 818.

[18] J.F. Nie, K.S. Shin, and Z.R. Zeng, Microstructure, deformation, and property of wrought magnesium alloys, *Metall. Mater. Trans. A*, 51(2020), No. 12, p. 6045.

[19] M.Z. Bian, Z.R. Zeng, S.W. Xu, W.N. Tang, C.H.J. Davies, N. Birbilis, and J.F. Nie, Enhanced tensile properties of Mg sheets by a unique thermomechanical processing method, *Metall. Mater. Trans. A*, 47(2016), No. 12, p. 5709.

[20] Z.R. Zeng, M.Z. Bian, S.W. Xu, C.H.J. Davies, N. Birbilis, and J.F. Nie, Effects of dilute additions of Zn and Ca on ductility of magnesium alloy sheet, *Mater. Sci. Eng. A*, 674(2016), p. 459.

[21] F. Vollertsen, Metal forming: Microparts, [in] K.H.J. Buschow, R.W. Cahn, M.C. Flemings, B. Ilschner, E.J. Kramer, S. Mahajan, and P. Veyssière, eds., *Encyclopedia of Materials: Science and Technology*, 2nd ed., Elsevier, Oxford, 2001, p. 5424.

[22] C.F. Gu, *Micro-Forming and Grain Refinement: Effects of Microstructural and Geometric Scale on Metal Formability* [Dissertation], Monash University, 2010.

[23] T. Nakata, C. Xu, Y. Uehara, T.T. Sasaki, and S. Kamado, Origin of texture weakening in a rolled ZEX4101 alloy sheet and its effect on room temperature formability and tensile property, *J. Alloys Compd.*, 782(2019), p. 304.

[24] M.Z. Bian, Z.R. Zeng, S.W. Xu, S.M. Zhu, Y.M. Zhu, C.H.J. Davies, N. Birbilis, and J.F. Nie, Improving formability of Mg–Ca–Zr sheet alloy by microalloying of Zn, *Adv. Eng. Mater.*, 18(2016), No. 10, p. 1763.

[25] T.T. Sasaki, F.R. Elsayed, T. Nakata, T. Ohkubo, S. Kamado, and K. Hono, Strong and ductile heat-treatable Mg–Sn–Zn–Al wrought alloys, *Acta Mater.*, 99(2015), p. 176.

[26] J.R. TerBush, N. Stanford, J.F. Nie, and M.R. Barnett, Na partitioning during thermomechanical processing of an Mg–Sn–Zn–Na alloy, *Metall. Mater. Trans. A*, 44(2013), No. 11, p. 5216.

[27] J.L. Li, X.X. Wang, N. Zhang, D. Wu, and R.S. Chen, Ductility drop of the solutionized Mg–Gd–Y–Zr alloy during tensile deformation at 350 °C, *J. Alloys Compd.*, 714(2017), p. 104.

[28] T. Hase, T. Ohtagaki, M. Yamaguchi, N. Ikeo, and T. Mukai, Effect of aluminum or zinc solute addition on enhancing impact fracture toughness in Mg–Ca alloys, *Acta Mater.*, 104(2016), p. 283.

[29] F.J. Humphreys and M. Hatherly, *Recrystallisation and Related Annealing Phenomena*, 2nd ed., Elsevier, Oxford, 2004.

[30] Z.R. Zeng, M.R. Zhou, P. Lynch, F. Mompiou, Q.F. Gu, M. Esmaily, Y.M. Yan, Y. Qiu, S.W. Xu, H. Fujii, C. Davies, J.F. Nie, and N. Birbilis, Deformation modes during room temperature tension of fine-grained pure magnesium, *Acta Mater.*, 206(2021), art. No. 116648.

[31] H. Somekawa, D.A. Basha, and A. Singh, Deformation behavior at room temperature ranges of fine-grained Mg–Mn system alloys, *Mater. Sci. Eng. A*, 766(2019), art. No. 138384.